Schweizerische Eidgenossenschaft
Confédération suisse
Confederazione Svizzera
Confederaziun svizra

Federal Department of the Environment, Transport, Energy and Communications DETEC

Swiss Federal Office of Energy SFOE
Energy Research and Cleantech Division

Final report dated 31.08.2023

HYSTIMATOR

Automated online hysteresis estimation for improved state estimation for LFP batteries

Source: ©CSEM 2023

Date: 30.08.2023

Location: Neuchâtel

Publisher:
Swiss Federal Office of Energy SFOE
Energy Research and Cleantech
CH-3003 Bern
www.bfe.admin.ch

Subsidy recipients:
CSEM SA
Rue Jaquet-Droz, 1, CH-2000 Neuchâtel
www.csem.ch

Authors:
Guillaume Thenaisie, CSEM, guillaume.thenaisie@csem.ch
Claudio Brivio, CSEM, claudio.brivio@csem.ch
Andreas Hutter, CSEM, andreas.hutter@csem.ch

SFOE project coordinators:
Stefan Oberholzer, stefan.oberholzer@bfe.admin.ch

SFOE contract number: SI/502441-0

The authors bear the entire responsibility for the content of this report and for the conclusions drawn therefrom.

Summary

The HYSTIMATOR project targets to improve state-of-charge (SoC) estimation for LFP cell chemistries. SoC estimation for LFP batteries is difficult due to a flat OCV curve and an important hysteresis effect. The Hystimator algorithm proposes to use electrochemical impedance spectroscopy (EIS) to incorporate hysteresis characteristics withing a physics-based Electric Circuit Model (ECM), which is validated with time domain lab measurements.

Zusammenfassung

Das HYSTIMATOR-Projekt zielt darauf ab, die Schätzung des Ladezustands (SoC) für LFP-Zellen zu verbessern. Die SoC-Schätzung für LFP-Batterien ist aufgrund einer flachen OCV-Kurve und eines wichtigen Hysterese-Effekts schwierig. Der Hystimator-Algorithmus schlägt vor, die elektrochemische Impedanzspektroskopie (EIS) zu nutzen, um die Hystereseeigenschaften in ein physikalisch basiertes elektrisches Schaltkreismodell (ECM) einzubeziehen, das mit Labormessungen im Zeitbereich validiert wird.

Résumé

Le projet HYSTIMATOR vise à améliorer l'estimation de l'état de charge (SoC) pour les piles LFP. L'estimation de l'état de charge des batteries LFP est difficile en raison d'une courbe OCV plate et d'un important effet d'hystérésis. L'algorithme Hystimator propose d'utiliser la spectroscopie d'impédance électrochimique (EIS) pour incorporer les caractéristiques d'hystérésis dans un modèle de circuit électrique (ECM) basé sur la électrochimique, qui est validé par des mesures de laboratoire dans le domaine temporel.

Sommario

Il progetto HYSTIMATOR mira a migliorare la stima dello stato di carica (SoC) per le batterie LFP. La stima del SoC per le batterie LFP è difficile a causa di una curva OCV piatta e di un importante effetto di isteresi. L'algoritmo Hystimator propone di utilizzare la spettroscopia di impedenza elettrochimica (EIS) per incorporare le caratteristiche di isteresi in un modello di circuito elettrico (ECM) basato sull’elettrochimica, convalidato con misure di laboratorio nel dominio del tempo.

Main findings

Based on recent advances in non-equilibrium thermodynamics, a new approach to the modelling of the hysteresis of LiFePO4 is proposed. A method for characterizing the hysteresis based on electrochemical impedance spectroscopy (EIS) is presented, which allows to reduce the characterization time from multiples weeks to few days. The results show that hysteresis in LiFePO4 is a very slow relaxation process strongly correlated with prior works results in crystalline phase transitions. An Electrical Circuit Model (ECM) of the cell is then extracted by using the distribution of relaxation times (DRT) on the EIS profile of the cell. The extracted DRT parameters show good agreement at low frequencies with previous thermodynamic studies. The performance of the ECM is compared with state of art physics-based ECM (without hysteresis compensation) for both fresh and aged cells. The result show an RMSE reduction of two to four folds depending on the tested cycling profile.

Contents

Abbreviations

DoD	Depth of Discharge
LFP	Lithium Iron Phosphate
SoC	State of Charge
SoH	State of Health
SoR	State of Resistance
ESS	Energy Storage System
EV	Electric Vehicle
OCV	Open Circuit Voltage
BMS	Battery Management System
ECM	Electric Circuit Model
GITT	Galvanostatic Intermittent Titration Technique
DRT	Distribution of Relaxation Times
CC	Coulomb Counting
DRT	Distribution of Relaxation Times
EIS	Electrochemical Impedance Spectroscopy
NMC	Lithium Nickel Manganese Cobalt Oxide (LiNiMnCoO2)
RMSE	Root Mean Square Error

1 Introduction

1.1 Background information and current situation

Pushed by the energy transition policies, EV adoption has exploded recently, representing close to 9% of the global car market[1]. Thanks to the stiff increase of raw materials costs and decent performances, LFP chemistry use in EV increased as well. Moreover, cells used in EVs, are often repurposed in ESS for second-life application[2], anchoring LFP for the next decades in the battery field.
Despite its popularity, SoC estimation, remains a challenge for LFP batteries[3,4]. This is explained by two main factors; firstly unlike other lithium chemistries
LFP displays a very flat SoC-OCV curve which leads to significant SoC computation errors, even with almost perfect OCV estimation[5]. Secondly, LFP chemistry displays a very strong hysteresis between the charging and discharging conditions, which deeply affect the precision of OCV tracking routines[6]. To address the limitation in lithium batteries, a common method is to use a Coulomb Counter (CC) that integrates the current to estimate the SoC. However, due to the imprecise integrated current sensor, frequent resets of the counter are necessary using SoC-OCV relationship[7,8]. In LFP, the flat OCV curve and hysteresis further reduce reset precision. Additionally, if one factors in the dependencies of OCV towards temperature and aging which are both nonlinear and inter-related, then the SoC estimation can no longer be considered as simple as it could be for other chemistries. Multiples attempts have been made to solve this issue [9,10,11]. They can be divided into two categories: empirical and data-driven modelling.
The empirical modelling approaches usually rely on the measurement of the hysteresis phenomenon as a function of SoC[12], sometimes with the addition of battery current or temperature[6], and in rare occasions the aging of the cell is discussed[11]. While this class of methods provide a straight-forward and conceptually easy way to model hysteresis, the non-linearities in the relationships between the OCV curves and the parameters requires an unworkable amount of data and computations to be done by the

---

[1] *L. Paoli and T. G ̈ul, "Electric cars fend off supply challenges to more than double global sales," E. IEA, 2022*

[2] *A. Colthorpe, "Wartsila claims 48mwh netherlands bess will be europe's first large-scale lfp battery project," energy storage news, December 2021*

[3] *R. Z. et al., "State of the art of lithium-ion battery soc estimation for electrical vehicles," Energies, vol. 11, Jul 2018*

[4] *Y. Zheng, M. Ouyang, X. Han, L. Lu, and J. Li, "Investigating the error sources of the online state of charge estimation methods for lithium-ion batteries in electric vehicles," J. Power ources, vol. 377, p. 161–188, February 2018*

[5] *A. Barai, W. D. Widanage, J. Marco, A. McGordon, , and P. Jennings, "A study of the open circuit voltage characterization technique and hysteresis assessment of lithium-ion cells," J. Power Sources, vol. 295, November 2015*

[6] *A. B. et al., "The influence of temperature and charge-discharge rate on open circuit voltage hysteresis of an lfp li-ion battery," IEEE Transportation Electrification Conference and Expo (ITEC), 2016.*

[7] *R. Xiong, Q. Y. J. Cao, H. He, and F. Sun, "Critical review on the battery state of charge estimation methods for electric vehicles," IEEE Access, vol. 6, 2018.*

[8] *R. Z. et al., "State of the art of lithium-ion battery soc estimation for electrical vehicles," Energies, vol. 11, 2018*

[9] *Y. H. et al., "Modeling of dynamic hysteresis characters for the lithium-ion battery," J. Electrochem. Soc., vol. 167, January 2020.*

[10] *J. Xie, J. Ma, Y. Sun, and Z. Li, "Estimating the state-of-charge of lithium-ion batteries using an h-infinity observer with consideration of the hysteresis characteristic," J. Power Electron., vol. 16, March 2016*

[11] *V. Ovejas and C. A., "Effects of cycling on lithium-ion battery hysteresis and overvoltage," Sci Rep, vol. 9, 2019.*

[12] *V. J. Ovejas and A. Cuadras, "Effects of cycling on lithium-ion battery hysteresis and overvoltage," Sci. Rep., vol. 9, December 2019.*

BMS. Furthermore, these curves are dependent on both the variations between batches of cells and the aging conditions which differ from cell to cell, leading to the need of regular calibration of the hysteresis. The data-driven modelling emerged as soon as battery databases got structured. Algorithms started to be trained to provide hysteresis estimators[13,14,15]. However, these algorithms suffer from a known limitation: (i) there is little warranty that a trained set of cells can be generalized to other cells, and (ii) the amount of data required for training might delay the time-to-market for a BMS solution.

1.2 Purpose of the project

Precise and robust SoC estimation is the basis for an optimal operation of battery assets. The project specifically targets SoC estimation, and the associated short-term objective is to provide a suitable hard- and software BMS solution for LFP batteries. This will allow to run battery assets in an optimal way and provide for instance a better estimation of the available driving range for LFP-powered EVs or more optimal use of ESSs.

As anticipated in section 1.1, the current state of art is deemed unsatisfactory, and an innovative approach is required. In this project, a physic-based approach of hysteresis is studied and modelled.

1.3 Objectives

This project proposes a physical-based method for addressing hysteresis by developing a phsyics-based model using EIS. An ECM is derived from the model and compared with a state-of-the-art physics-based mode lacking hysteresis compensation. The KPI adopted to compare the different models' performances (hystimator vs. literature) is the calculation RMSE w.r.t the measurements.

2 Procedures and methodology

The methodology started from the LFP electrochemical fundamental, moved then on how EIS can be used to model the hysteresis phenomenon (e.g. how to extract useful parameters from EIS to model the hysteresis).

2.1 Theory of LPF electrochemistry

Hysteresis is a macro phenomenon that can be found in various field of science, and which is characterized by the "dependence of the state of a system on its history". In the current case, hysteresis translates by different values of OCV depending on the fact that the cell was charging or discharging prior to the relaxation that led to the measurement.

Early works in non-equilibrium thermodynamics have shown that in LFP, the ion intercalation process is not as straightforward as in other lithium-based chemistries[16]. Further works demonstrated that the electrode must undergo partial reconfiguration of the triphylite lattice to accept Li+. The study of the

[13] *Farrokh, D. M., F.S., Dizaji, and M. Hysteresis, "Identification using extended preisach neural network," Neural Process Lett, vol. 54, 2022.*

[14] *Z. Chen, S. Qiu, M. Masrur, and Y. L. Murphey, "Battery state of charge estimation based on a combined model of extended kalman filter and neural networks," in The 2011 International Joint Conference on Neural Networks, 2011, pp. 2156–2163*

[15] *M. Trapanese, V. Franzitta, and A. Viola, "The jiles atherton model for description of hysteresis in lithium battery," in 2013 Twenty-Eighth Annual IEEE Applied Power Electronics Conference and Exposition (APEC), 2013, pp. 2773–2775.*

[16] *D. Morgan, z A. Van der Ven, and G. Ceder, "Li conductivity in lixmpo4 m = mn, fe, co, ni olivine materials," Electrochemical solid state letters, 2004*

lattice showed that Li+ have a single direction of progress inside the lattice along the plan (0,0,1)[17]. This causes a wave of local phase transition triggered by the nearby ionic potential, which lead to a macro intercalation following a surface diffusion model. This is a two steps relaxation process could take a longer time than a simple intercalation, due to the time constant of the lattice transformation, and the time constant of the ionic movement inside the lattice.

However, study on real crystal, where vacancies can be occupied by impurities, showed that Li+ can also diffuse along (1,0,0) and (0,1,0) rather than only mono-dimensionally, following a bulk diffusion model rather than a surface diffusion model (Fig 1)[18]. In this case, a third time constant due to the bulk diffusion is is also contributing to the intercalation process. Moreover, it was reported that in LFP, the surface diffusion is one order of magnitude faster than the ionic diffusivity, which in turn is two orders faster than the bulk diffusion.

Therefore, this work proposes as a guiding hypothesis that hysteresis in LFP is not an intrinsic phenomenon, but rather a much slower relaxation than other chemistries.

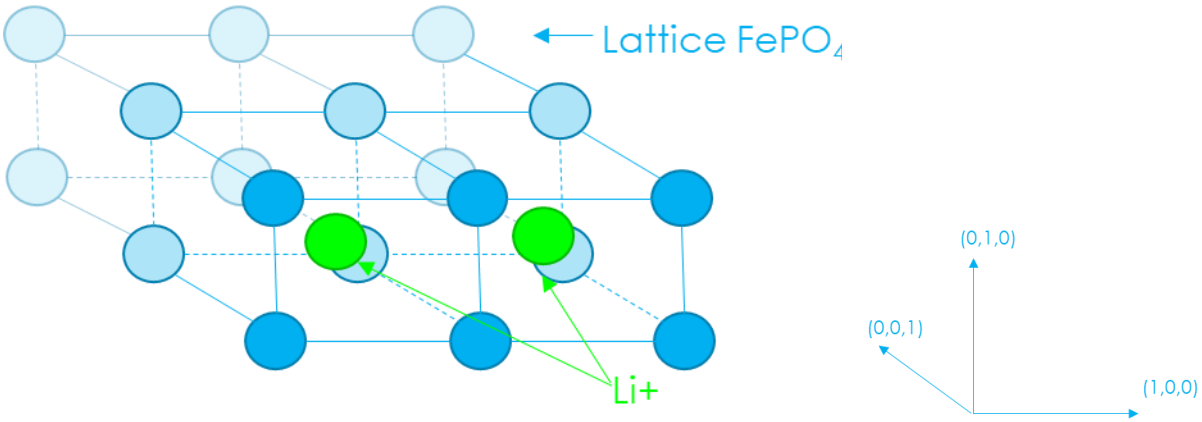

Fig 1: bulk diffusion model for LFP chemistry as proposed in [18].

2.2 EIS for hysteresis model parameters extraction

Integrating a complex electrochemical modelling of the relaxation (such as shown in [4], [11], [12]) in a classical SoC estimation algorithm is hardly realistic due to the high number of inter-related parameters that force trade-offs between precision and computation/memory cost. Instead, this works proposes to approximate this relaxation with a RC network matching the hysteresis time-constants anticipated in the previous section, which can be integrated in a conventional ECM. Usually, the characterization of ECM parameters is done by Galvanostatic Intermittent Titration Technique (GITT). However, given the presence of hysteresis, this would require weeks of experiment, which is not compatible with the needs of a BMS to update the ECM while battery is aging. Another method would consist in reducing the GITT rest time, to fit a relaxation model to the curve, and then to deduce the final OCV value. However, since a significant part of the full relaxation will be not measured, an accurate behavioural model will be needed to properly extrapolate the final voltage. This would require a prior characterization of the cell, which would limit the online applicability in BMS. Thus, this work proposes to: (i) extract the EIS of the

[17] *M. Z. Bazant, "Theory of chemical kinetics and charge transfer based on nonequilibrium thermodynamics," Acc. Chem. Res, 2013*

[18] *Hong, L., Li, L., Chen-Wiegart, YK. et al. Two-dimensional lithium diffusion behavior and probable hybrid phase transformation kinetics in olivine lithium iron phosphate. Nat Commun 8, 1194 (2017).*

cell once, at extremely low frequencies, (ii) to use the previous work [19,20] to deconvolute the impedance and, (ii) to extract the parameters of the intercalation process by making extensive use of DRT.

2.3 Low frequency, bias-free EIS

To perform an DRT, the impedance must be measured over the frequency range of interest [18]. EIS is to be performed under conditions where the cell can be considered as a linear system. However, when performing EIS at very low frequencies, the amount of charge stored and retrieved in the cell during a half period of the sine wave is no longer negligible. This leads to a change of the cell's OCV. On a small evolution of SoC, one can assume OCV to linearly change in consequence. Therefore, as shown in Fig 2, the OCV increases during positive half-period of the wave and decreases during the negative half-period. The lower the frequency, the more significant the OCV changes, and the less linear the cell.

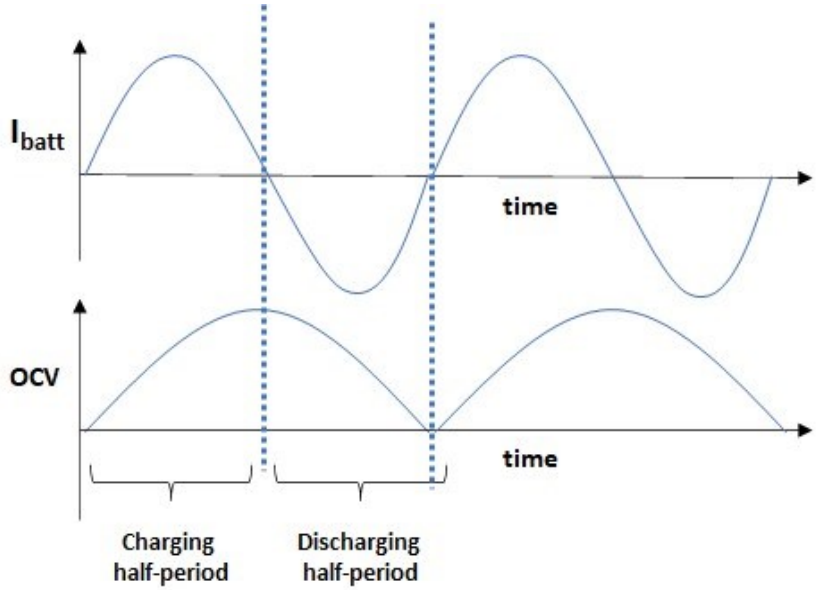

Fig 2: Change of OCV during a galvanic sine

To determine the frequency below which the OCV must be factored in, the following steps are followed:

1. The function $OCV = f(SoC)$ is extracted by GITT.
2. The impedance is extracted in lab down to 10 mHz (limit of regular EIS).
3. A synthetic current wave is built for each frequency of interest.
4. The change of SoC during the sine wave is computed following Eq (1). And the change of OCV is determined from the function of Step 1.
5. The change of voltage of the cell due to the ohmic effect is computed by using Ohm's law and the value of impedance for the frequency of interest. Below 10 mHz, the value of the 10 mHz impedance is used. It is false but to obtain an order of magnitude it is deemed reasonable.
6. The resulting battery voltage is obtained by adding the change of OCV of the Step 4 and the Ohmic voltage of Step 5.

[19] *P. Iurilli, C. Brivio, R. E. Carrillo, and V. Wood, "Eis2mod: A drt-based modeling framework for li-ion cells," IEEE Transactions on Industry Applications, vol. 58, no. 2, pp. 1429–1439, 2022.*

[20] *P. Iurilli, C. Brivio, and V. Wood, "Detection of lithium-ion cells' degradation through deconvolution of electrochemical impedance spectroscopy with distribution of relaxation time," Energy Technology, 2022*

$$Q = \int_0^{\frac{T}{2}} I \cdot sine(t) \cdot dt \tag{1}$$

Where Q is the capacity charged (resp. discharged) from the cell, I is the amplitude and T the period of the sinewave.

Examples of the obtained synthetic battery voltages are shown in Fig 3 for some frequencies below 1mHz. It can be seen that from 0.5 mHz, the response of the cell is no longer a mono-harmonic sine, but that the OCV drift starts to distort it. Thus, for sub mHz frequencies, a correction is even more required.

An approach based on the use of the Lissajous plot is proposed. In case of a linear system such a plot is expected to be elliptic or a straight line. A synthetic Lissajous plot is constructed using one of the previously obtained voltages in Fig 3. In Fig 4-left, a synthetic plot shows both the ideal plot (green dots) and distorted plot (blue line) without and with OCV effect. It can be observed that the ideal ellipsis (without OCV effect) is inside the distorted Lissajous plot (with OCV effect). Thus, it is proposed to perform an ellipsis fitting while respecting the maximum area of the real Lissajous plot and extract the actual impedance from the measured data.

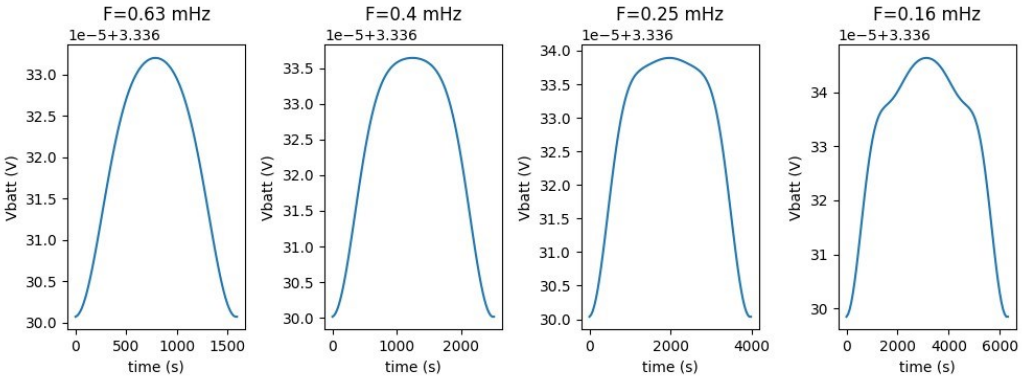

Fig 3: Effect of OCV over a sine wave of current at low frequencies.

The finding of the ellipsis belongs to the convex optimization class of problem and is described in details in existing repositories[21]. The problem is stated as follow:

"Given a point cloud containing points v_1, ..., v_n, we want to find a large ellipsoid satisfying:

- The ellipsoid is contained within the convex hull of the point cloud.
- The ellipsoid doesn't contain any of the point v_i in the point cloud.

To find such an ellipsoid, we solve a sequence of semidefinite programming problems."

The ellipsis is parametrized as:

$$E = \{x | x^T P x + 2q^T x < r\} \tag{2}$$

[21] Hongkai-Dai, "Find a large inscribed ellipsoid", Github link.

where P,q,and r are unknowns. The condition that the ellipsoid doesn't contain any of the points v_i can be expressed as the following constraint:

$$\forall i \in [0,n], vi \notin E \iff vi^T Pvi + 2q^T vi \geq r \tag{3}$$

If the convex hull of v_i is describe as the polytope

$$\forall i \in [0,n], \qquad ConvexHull(vi) = \{x | Cx \leq d\} \tag{4}$$

Using the s-lemma[22] we know that the ellipsoid is within the convex hull if and only if

$$E \in ConvexHull(vi) \Leftrightarrow \exists \lambda i \geq 0, such\ that \begin{bmatrix} P & 1 - \frac{1}{2}\lambda ici \\ \left(q - \frac{1}{2}\lambda ici\right)^T & \lambda idi - r \end{bmatrix} \succcurlyeq 0 \tag{5}$$

Where c_i, di is the i'th row of C, d respectively. $\succcurlyeq 0$ means that the matrix is positive semi-definite.
To guarantee that the quadratic function $x^T Px + 2q^T x \leq r$ describes an ellipsoid (not other shapes like a hyperbola), we require the following two conditions:

$$P \succcurlyeq 0 \tag{6}$$

$$\exists z, such\ that\ z^T Pz + 2q^T z \leq r \tag{7}$$

Thus, to maximize the ellipsoid, we can maximize the logarithm of

$$max\ n\ log(r + q^T P^{-1} q) - log\ det(P) \tag{8}$$

The general idea is to solve the non-convex optimization problem iteratively. In each iteration the objective is linearized and the convex optimization problem within a trust region is solved.
The detail of the algorithm is provided in the code repository[20].

The resulting algorithm is applied to the synthetic data in Fig 4-left: the overlap between the ideal Lissajous (no OCV effect) and the reconstructed show the goodness of the method.

Fig 4-right show the application of the method with the experimental data obtained at 10 uHz. This method will be used to reconstruct a "clean" EIS from the distorted measurements.

[22] Olik, I. Terlaky T." A Survey of the S-Lemma," SIAM Review, vol. 49(3):371-418, 2007.

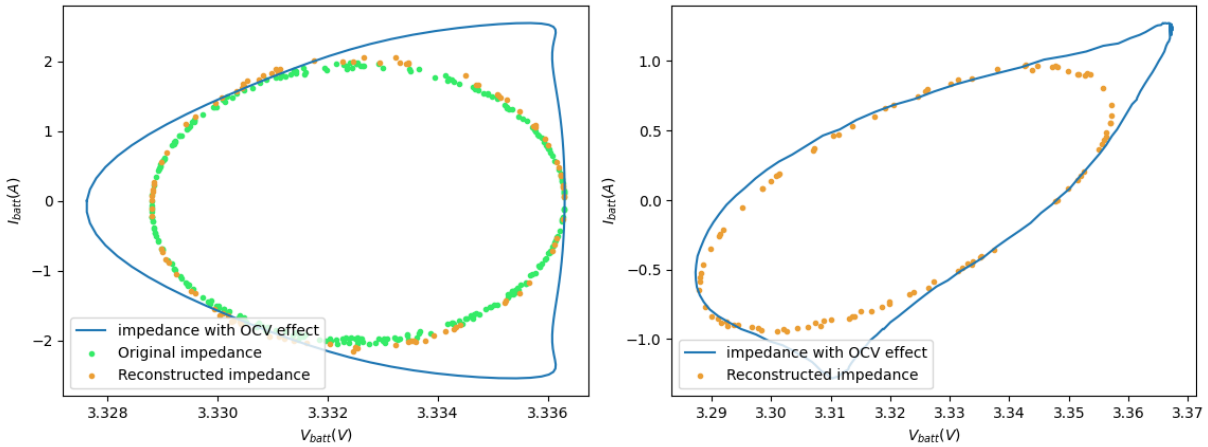

Fig 4: Synthetic and measured Lissajous curves at 10 uHz.

(left) Synthetic Lissajous plot with and without OCV-induced effect, (right) measured Lissajous plot with reconstructed one

2.4 ECM configuration

Previous analyses in [19] proposed building an ECM by deconvoluting the EIS curve using the DRT method. However, hysteresis was not discussed in the prior work, which focused on NMC cells and approximated low frequencies using a Warburg element. This study extends the DRT to low frequencies to deconvolve the EIS and obtain relaxation time that matches the physics-based assumption of previous section II.A. The ECM's R(s) and C(s) values extraction process works as follow:

1. The peak characteristics of relaxation times are identified from the obtained DRT. The centre value of each peak providing the time constant.
2. An R-C element is associated to each time constant.
3. The function least squares from the Python library *Scipy.interpolate* is used to perform the fitting of the measured EIS and to extract the values of each R(s) and C(s) of the ECM. The algorithm is initialized as follow:
    a. The initial R value is determined by dividing the measured IR drop of the cell during GITT by the number of R-C networks.
    b. The initial values of C are determined from the resistance and the time constant.

3 Experimental analysis

The testing campaign has been performed at the CSEM's Sustainable Energy Center, Neuchatel (Switzerland) on several 90 Ah LFP cell under controlled condition with testing set-up composed of:

1) A cell tester Biologic BCS815 equipped with 32 parallel, 9V/15A channels (0.01% FSD accuracy on the voltage and 0.015% FSD accuracy on current, for each available range) with EIS spectroscope multiplexed and able to range from 10 kHz to 10 mHz.
2) A thermostatic chamber ATT-DM1200T with 45◦ C–180◦ C temperature range.
3) Potentiostat/galvanostat Gamry reference 3000 for EIS measurements in the range from 1 MHz to 10 µHz,

A total of five LFP cells (images of the cells under tests can be found on the cover photo of this report) have been tested with different type of protocols. Here below, a summary of the tests that each cell underwent:

Cell HYST_1_1 (referenced as AGED cell in the following)
i. Cycling: cycled 1C/1C for 1000 cycles.
ii. GITT 10h relaxation
iii. Dynamic profile @ SoCs:85%-50%-15%
iv. EIS (10kHz – 100uHz)

Cell HYST_2_2 (referenced as FRESH cell in the following)
i. GITT 1h relaxation
ii. Dynamic profile @ SoCs:85%-50%-15%

Cell HYST_2_3 (referenced as FRESH cell in the following)
iii. GITT 10h relaxation

Cell HYST_2_4 (referenced as FRESH cell in the following)
i GITT 5h relaxation
ii EIS (10kHz – 10mHz) repeated with several excitation currents

Cell HYST_2_5 (referenced as FRESH cell in the following)
i 5 days relaxation
ii EIS (10kHz – 10uHz)

In total, it is estimate that the overall test took roughly about 277 days of testing resources. The full test list is shown in the appendix.

3.1 Analysis of the hysteresis phenomenon

An LFP cell (cell HYST_2_5) has been studied under controlled conditions. The cell was placed in the temperature chamber and linked to the battery tester. The cell was charged to 3.6V using a CC-CV method, left to rest for over 24 hours to ensure that the thermal equilibrium would be reached, then a current pulse of C/10 for 30 minutes was applied and released, finally the voltage of the cell was monitored over few days. The result are plotted in Fig 5. It can be seen that unlike other chemistries (NMC, lco, etc.), the relaxation of LFP is 2 to 3 orders of magnitude slower (e.g. NMC is in the orders of 10^0 hours and LFP in the order of 10^2 hours). This induces a clear difference in voltage measured under charge or discharge conditions.

In the meanwhile, another LFP cell (cell HYST_2_3) was measured by GITT, with a relaxation of 10 hours at each step. From each relaxation step, the cell voltage was measured after 3, 5, 10, hours relaxation. Fig 6 displays the results, which demonstrate the validity of the initial hypothesis regarding the nature of the hysteresis (i.e. hysteresis is a slow relaxation phenomenon) and prove that the results from GITT (and similar methods) provide only pseudo-OCV. Additionally, it can be observed that the relaxation speed is not uniform over the full SoC range, leading to significant errors in the computation of standard of SoC-OCV lookup table.

To reduce the SoC estimation error and accurately characterize the full relaxation process, extracting both OCV and relaxation parameters with high precision is essential. While GITT is the most obvious method, it requires waiting for the relaxation to complete and results in half a week of monitoring for each step, as demonstrated by Fig 5, which makes it impractical for a BMS application. On the contrary,

the use of EIS at low-frequency EIS requires only a few days and it can provide the same information as a GITT conducted over several weeks.

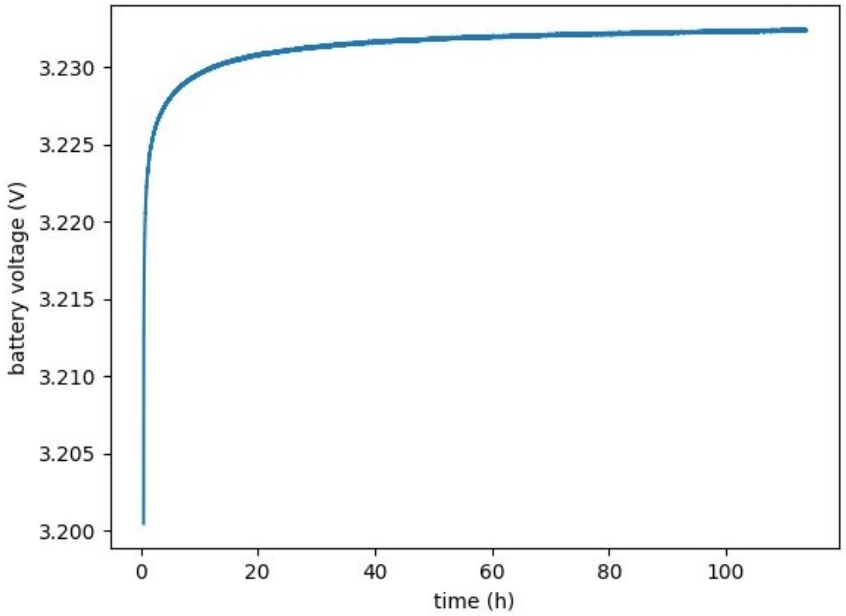

Fig 5: Relaxation of a FRESH 90 Ah LFP following a C/10 30 minutes pulse over 6 days.

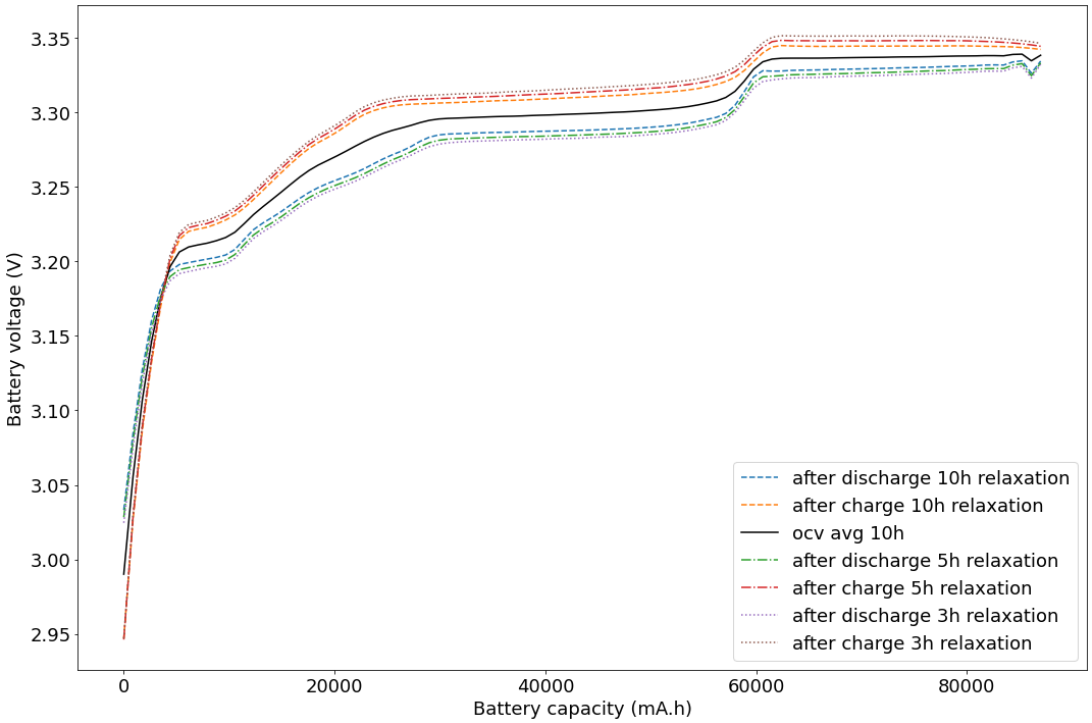

Fig 6: Pseudo-ocv curves obtained from a FRESH 90Ah LFP cells by large-current-steps GITT

3.2 EIS measurement and correction

An EIS was extracted from 1 kHz down to 10 μHz by using potentiostat/galvanostat Gamry reference 3000. The peculiar EIS shape of LFP cells at low frequencies is well-know in literature and mark the difference with other intercalation-based chemistries (NMC, NCA, etc.)[23]. The data is corrected accordingly to the method described in section 2.3, and the results are shown in Fig 7.

In the case of the aged cell, due to the limitation in time, the full spectrum was not extracted, and only the measurement down to 100uHz where performed. As expected, the impedance tends to increase with the aging of the cell.

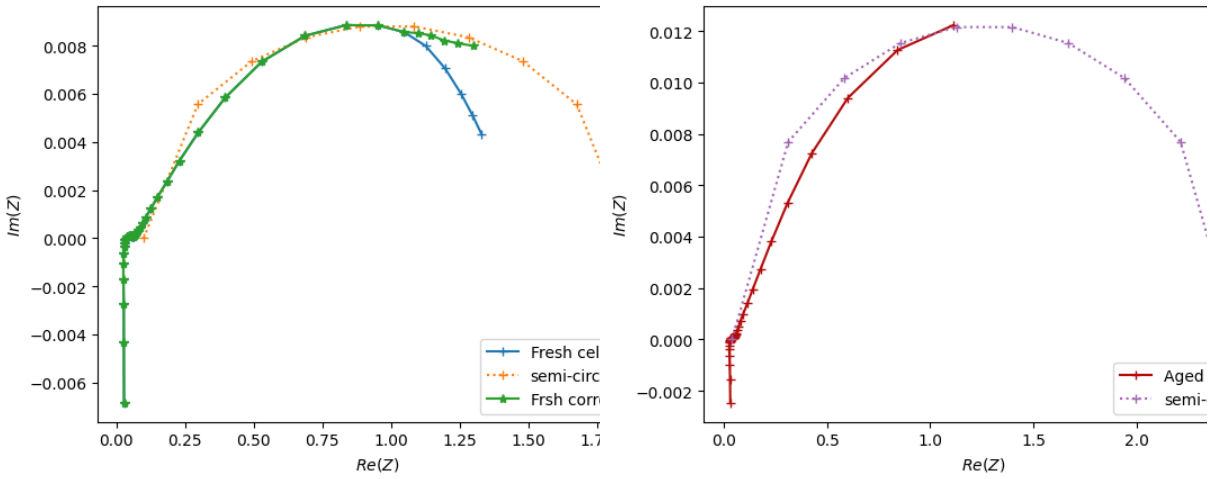

Fig 7: EIS of a 90Ah LFP cell (FRESH on the left and AGED on the right), measured from 1 kHz down to 10 μHz, 'raw' from the measurement equipment and corrected.

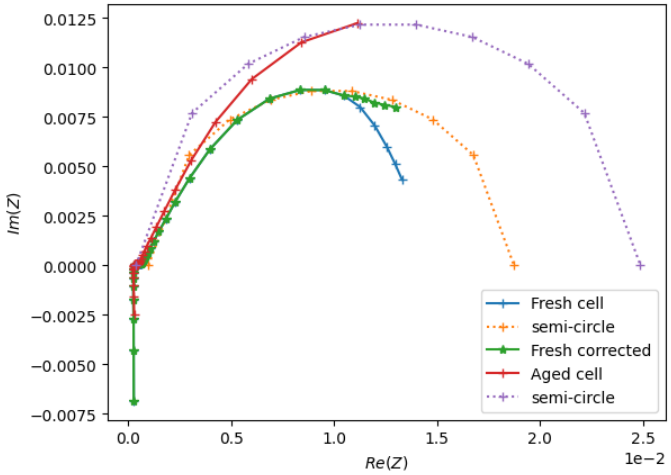

Fig 8: Comparison of ESI of LFP cells, FRESH vs. AGED.

[23] *J. Illig. et al. Understanding the impedance spectrum of 18650 $LiFePO_4$-cells. Journal of Power Sources 239, 670-679 (2013).*

3.3 ECM parameters extraction

The method described in sub-section 2.4 is applied to the corrected EIS, and the parameters of the ECM are extracted from DRT displayed in Fig 9 and shown in the Tab 1, for both fresh and aged cells.

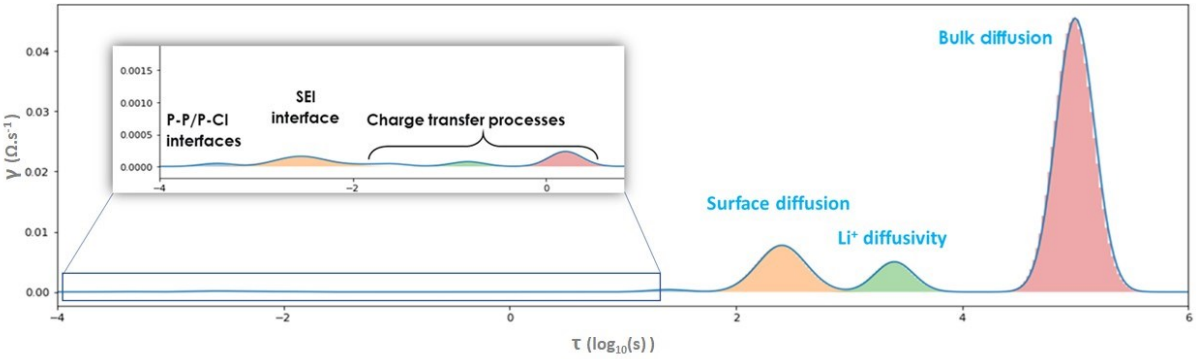

Fig 9: DRT of the studied 90Ah LFP FRESH cell. The figure is spread in 2 rows to display the dynamic range of the peaks.

Focusing on the fresh cells and as stated in section 2.1, 3 relaxation times were found at the lowest frequencies, thus corresponding to three distinct processes. The first having a relaxation time approximately 10 times smaller than the second, which in turn is 100 times shorter than the third. Therefore, it is proposed to assign these three peaks to the three identified phenomena. It should be noted that further validation through invasive/destructive tests is required to fully confirm the physical assignments. However, such tests are beyond the scope of this article.

Based on this electrochemical characterization assumptions for the fresh cell, the final ECM is thus composed of RCi with i(s) comprised from 1 to 7, as shown in Fig 10.

Tab 1: ECM parameters obtained after extraction by DRT and their physical attribution.

RC #	Physical meaning	Value(s) – fresh cell	Value(s) – aged cell
RC0*	P-P and P-Cl interfaces	3.78E-04	6.187e-04
RC1*	SEI interface	3.10E-03	4.533e-03
RC2*	Charge transfer process	1.1E-02	7.796e-02
RC3*	Charge transfer process	1.60E+00	
RC4*	Charge transfer process	1.51E-01	8.752e-01
RC5⁺	Surface diffusion	2.53E+02	3.740e+02
RC6⁺	Li+ diffusivity	2.47E+03	----------
RC7⁺	Bulk diffusion	9.90E+04	----------

* was demonstrated in [19], [20], + are proposed by this work.

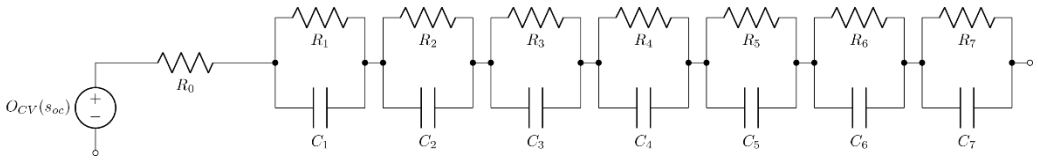

Fig 10: Final ECM selected to model LFP chemistry including the hysteresis

As regards of the aged cell analysis, EIS at frequencies below 100uHz was not performed due to safety. Consequently, the direct extraction of the last two peaks of the DRT was precluded. Nevertheless, it is postulated that the aging process has a less pronounced impact on lithium diffusivity, with surface diffusivity being more susceptible to aging effects compared to deep bulk diffusivity. Consequently, to estimate the values of the last two peaks, data from fresh cells were employed and extrapolated to the aged cell context. Although these values are recognized as suboptimal, they are deemed reasonable approximations under the current circumstances.

Notably, an intriguing observation was made concerning the merging of peaks 2 and 3 in the DRT analysis. This phenomenon can be attributed to the growth of one of the peaks, which eventually engulfs the other, making its detection challenging for the DRT algorithm. It is speculated that the RC2 peak might be the one primarily responsible for this merging, given its proximity to the same order of magnitude as the merged peak. This peculiar aging behavior has been previously reported[20], indicating that further in-depth post-mortem investigations are essential to propose a bullet-proof physical interpretation for this phenomenon, and enhance the accuracy of the model while ageing.

From Fig 10, the state equation of the system can be written as:

$$X_{k+1} = \begin{bmatrix} 1-\frac{-Ts}{R_1C_1} & \cdots & & 0 \\ \vdots & & & \vdots \\ \vdots & \ddots & & \vdots \\ \vdots & & 1-\frac{-Ts}{R_{11}C_{11}} & \vdots \\ \vdots & & & 1-\frac{-Ts}{R_{hys}C_{hys}} \quad 0 \\ 0 & \cdots & \cdots & 0 \quad 1 \end{bmatrix} \cdot X_k + \begin{bmatrix} \frac{Ts}{C_1} & \cdots & \frac{Ts}{C_{11}} & \frac{Ts}{C_{hys}} & \frac{Ts}{C_n} \end{bmatrix} \cdot I \tag{9}$$

where $X = \begin{bmatrix} V_1 \\ SOC \end{bmatrix}$, I the current in the battery, C_n the battery nominal capacity, and T_s the sampling rate. If the sampling is set to 1 second, the standard form of the state space function can be obtained as:

$$X_{k+1} = A_k \cdot X_k + B_k \cdot I_k \tag{10}$$

where $A_k = \begin{bmatrix} d_1 & \cdots & & 0 \\ \vdots & \ddots & & \vdots \\ \vdots & & d_{11} & \vdots \\ \vdots & & & d_{hys} \quad 0 \\ 0 & \cdots & 0 & 1 \end{bmatrix}$, $\forall i \in [1,11], d_i = 1 + \frac{1}{R_iC_i}$,

$d_{hys} = 1 + \frac{1}{R_{hys}C_{hys}}$

and $B = \left[\frac{-1}{C_1}; \ldots; \frac{-1}{C_{11}}; \frac{-1}{C_{hys}}; \frac{-1}{C_n}\right]$

With V_{batt} given by:

$$V_{batt} = h(X) + I \cdot R_0 \tag{11}$$

where $h(x) = \sum_{i=1}^{11} V_i + V_{hys} + OCV(SOC)$.

4 Results and discussion

The proposed ECM is compared with an existing model from literature[24], which was built for NMC cells by applying a similar methodology (e.g. DRT on the EIS of a li-ion cell with a frequency range of 10 mHz to 1 kHz). In the model, 6 RC elements were used to simulate a Warburg diffusion behavior at low frequencies, but without hysteresis compensation.

The averaged OCV was obtained from the GITT with a C/10 pulse and 10 hours of relaxation, either from the fresh or aged LFP cell by interpolating using a B-Spline of third order with functions splrep and splev from the Python library Scipy.interpolate..

In each simulation, the initial OCV was set by the measured cell voltage in relaxed condition from measurement, and it was assumed that every capacitors of the RCs networks were empty (battery fully relaxed).

Two different tests have been performed to validate the model in the time domain and its ability in simulating the voltage at the cell terminals:

1. *Square current profile tests*: to verify model accuracy in reproducing the solicitations deriving from fast square current profile (5 mins steps).
2. *GITT tests:* to verify the model accuracy at intermittent current with a full charge-discharge cycle, with longer relaxation periods.

The accuracy of the model is evaluated by means of the RMSE indicator (Python library ”sklearn”):

$$RMSE = \sqrt{\frac{\int_0^T \left(X_{measurements}(t) - X_{model}(t)\right)^2}{T}}$$

Where *X* is the terminal voltage.

4.1 Performance in response to dynamic profile

A dynamic profile (code name: DYN) was built which consists of a repetition of current pulses of increasing amplitudes (C/10, C/5, C/2) separated by 5 minute resting periods (Fig 11). The dynamic test was conducted at three different state-of-charge (SoC) levels: high (85%), medium (55%), and low (15%).

Tab 2: Comparison of RMSE values for proposed ECM and reference ECM (without hysteresis compensation).

DYN	Fresh cell		Aged cell	
SoC	Proposed ECM	Reference ECM	Proposed ECM	Reference ECM
85%	15.6 mV	70.5 mV	19.6 mV	68.5 mV
50%	14.3 mV	63.9 mV	20.3 mV	63.8 mV
15%	15.2 mV	65.3 mV	21.1 mV	64.2 mV

[24] *P. Iurilli, C. Brivio, R. E. Carrillo, and V. Wood, “Eis2mod: A drt-based modeling framework for li-ion cells,” IEEE Transactions on Industry Applications, vol. 58, no. 2, pp. 1429–1439, 2022.*

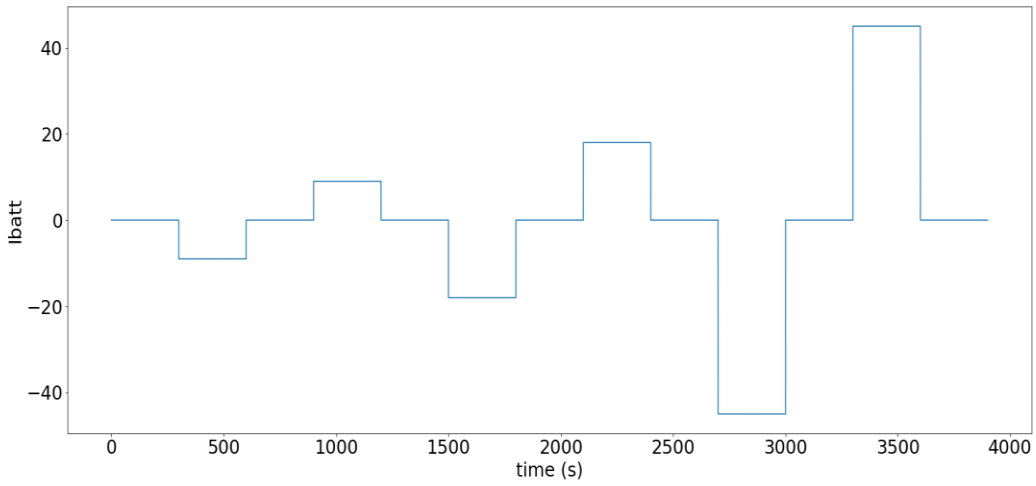

Fig 11: reference current profile applied in the dynamic tests.

The proposed model outperforms the reference model especially in the relaxation phases at the higher currents, where it converges towards a similar hysteresis-shifted value. The results of the comparison are displayed in Fig 12, which shows the performance of the proposed ECM and the reference one. It must be noted that the performances of the model are strongly dependent on the R(s)-C(s) extraction algorithm described in subsection 2.4: it has been observed that local minima could lead to erroneous RC values estimation which lead to strong divergence of the model from the measurements.

Overall, the proposed ECM demonstrated improved accuracy compared to the reference ECM across all SoC levels. It should be noted that the model parameters from EIS/DRT were extracted at 50% SoC, and therefore do not encompass SoC dependency. The RMSE values indicate that the proposed ECM achieved an estimation error around 15 mV (Tab 2), while the reference ECM had an estimation error around 65 mV, thus ~4 folds gain higher on average.

These results suggest that the proposed ECM is a promising method for accurately estimating the state-of-charge of LFP batteries.

When moving to the aged cells, the results shown in Fig 13 demonstrates that the proposed approach remains valid for aged cells and continues to provide superior estimations compared to the reference. However, it is noteworthy that the advantages obtained through the proposed approach diminish as the cell ages, with a reduction in gains to ~3 folds. This finding suggests that the low-frequency segment of the spectrum, previously hypothesized as relatively independent of aging effects, does indeed undergo changes with age, albeit to a lesser extent than other model parameters.

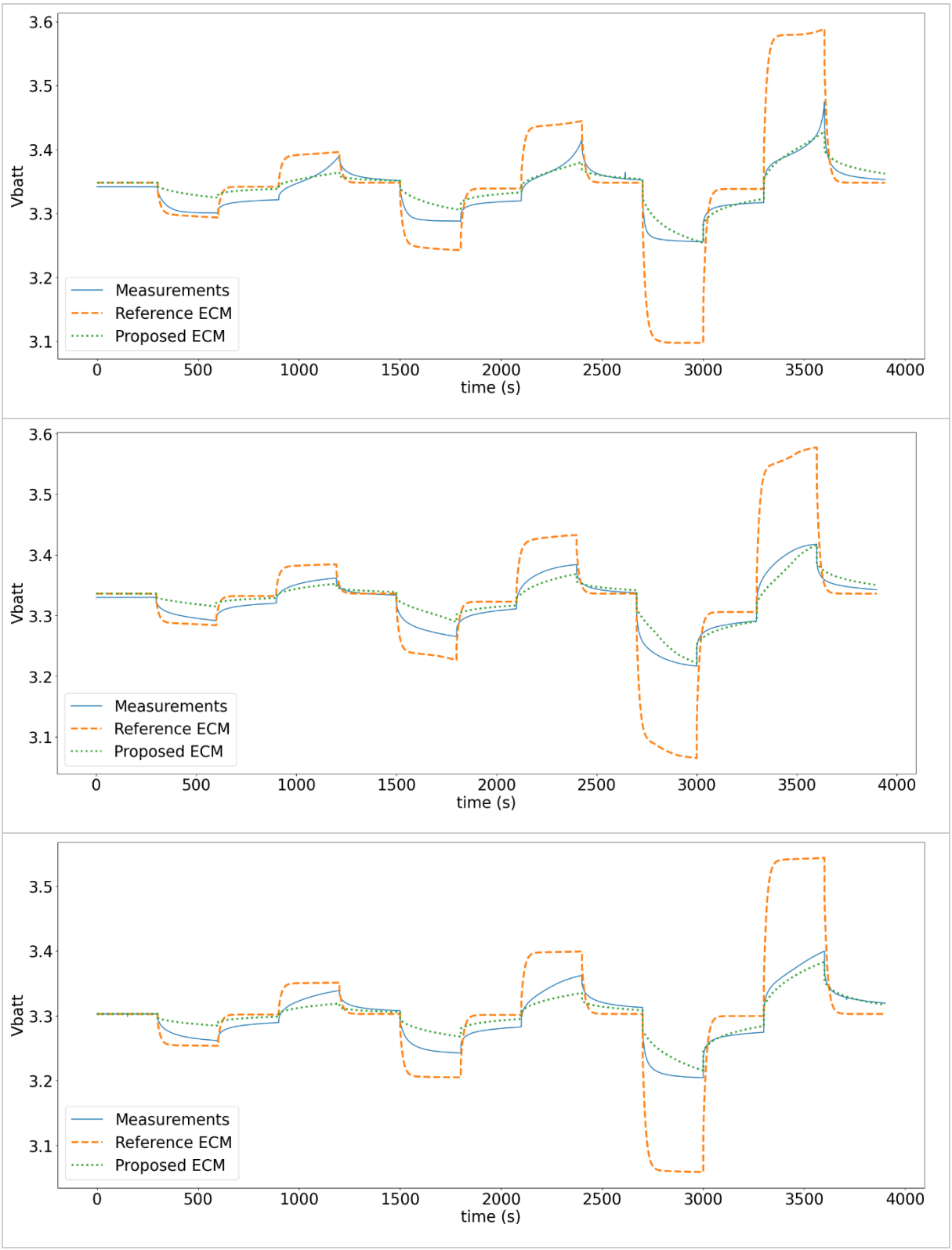

Fig 12: Comparison of the performances of the proposed ECM during dynamic cycling for a FRESH cell. From top to bottom: simulation results at SoC=85%, simulation results at SoC=50%, simulation results at SoC=15%,

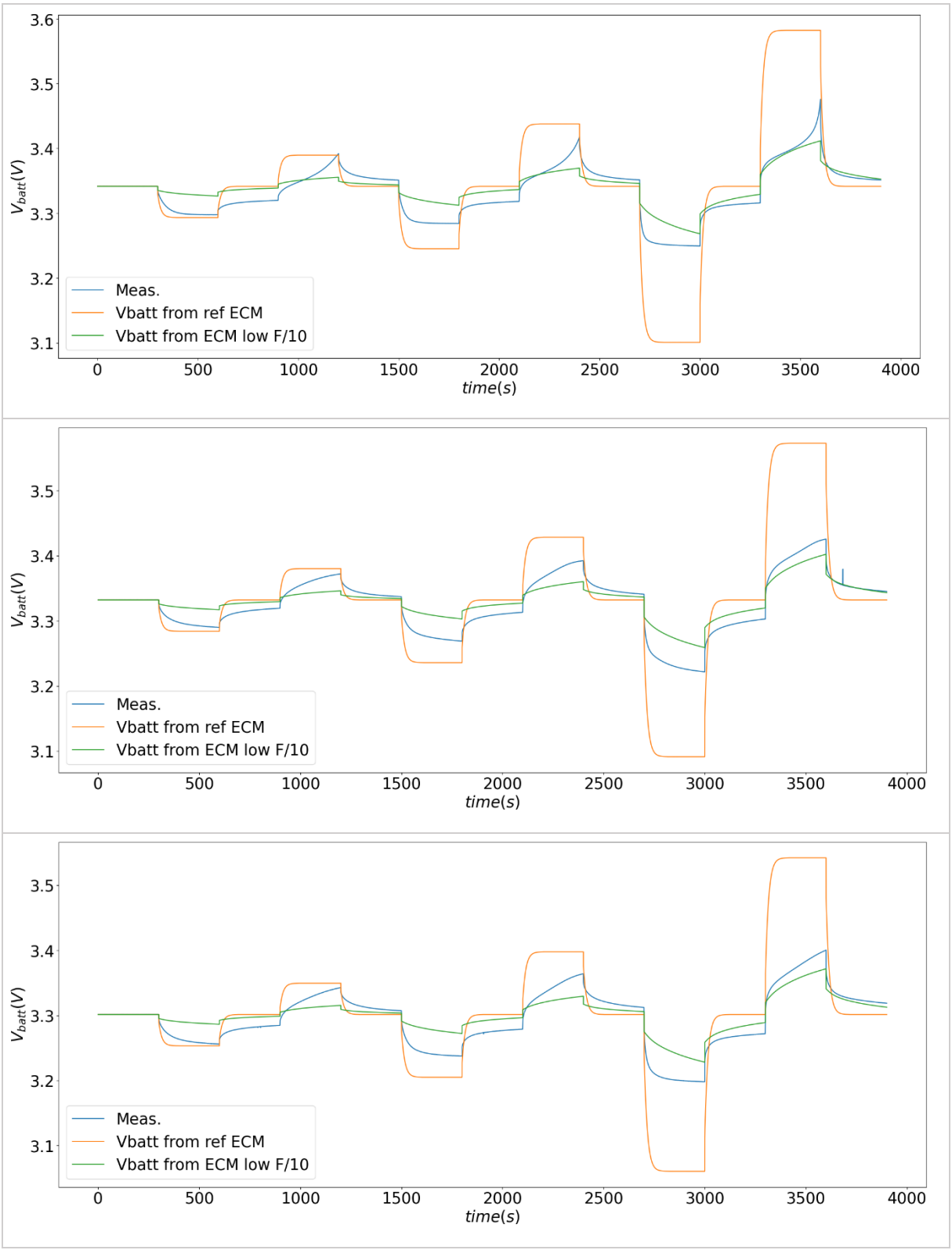

Fig 13: Comparison of the performances of the proposed ECM during dynamic cycling for an AGED cell. From top to bottom: simulation results at SoC=85%, simulation results at SoC=50%, simulation results at SoC=15%,

4.2 Performance in response to GITT profile

The GITT test was employed to assess the performance of the proposed ECM vs. reference model when full discharge/charge and long relaxation (10h) are accounted. Since these tests entails a full discharge/charge cycle with intermittent current at C/10, both the proposed and reference ECMs were used in conjunction with a lookup table and a coulomb counter to derive the OCV to be fed to the model. As shown in Fig 14 and Fig 15, The GITT protocol is slightly different between the fresh and aged cells. In the case of the fresh cell, current steps at C/10 were lasting 10 minutes, while in the case of the aged cell, the same current steps were imposed to last 1h to reduce the testing times.

The results of Tab 3 confirms that the proposed ECM outperforms the reference model also in this case, exhibiting approximately twice the improvement in RMSE. While the performance gain between the proposed and reference models was not as good as observed in the dynamic profile analysis (~ 2 fold), this outcome can be explained by the influence of OCV/SoC initialisation which could contribute to an overall average error. Additionally, extreme SoC values were observed to have a significant impact on the error, which can be explained by a significant difference of EIS measurements at extreme SoCs (SoC < 5% and SoC > 95%).

Aging effects were also evaluated in both the proposed and reference models. The results demonstrated that aging led to an increase in errors for both models. However, the rate of increase in error was approximately two times lower in the proposed model compared to the reference model. This observation further highlights the superior performance of the proposed ECM, as it exhibits greater resilience against the degrading effects of cell aging.

Tab 3: Simulation results over dynamic profile for proposed ECM vs. reference ECM (without hysteresis compensation).

RMSE	Fresh cell		Aged cell	
	Proposed ECM	Reference ECM	Proposed ECM	Reference ECM
GITT (10h)	43.3 mV	71.2 mV	90.7 mV	173.7mV

5 Conclusions

In this work, the goal was to characterize and model the hysteresis of LFP cells by using EIS. We proposed a modelisation based on physics-based principles from thermodynamics, which has shown that the intercalation in LFP is governed by a complex interaction between three main dynamics: surface diffusion, Li+ diffusivity and bulk diffusion. The resulting ECM model was built by applying DRT on the EIS spectra of the cell at very low frequencies (10 uHz) in order to characterize the time constant of these dynamics. The model was found to agree well with the measurements, and this was confirmed by the simulated results on both fresh and aged cells with.

Specifically, the proposed ECM demonstrated superior modelling capabilities compared to the reference model when subjected to dynamic current profile and full GITT charge/discharge cycles. The improved performance suggests that the proposed ECM could be effectively utilized in a Kalman filter or other estimators to enhance State of Charge (SOC) estimation accuracy. By leveraging the strengths of the proposed ECM and considering its enhanced performance and resilience to aging effects, this research contributes to advancing battery modelling techniques and lays the groundwork for more accurate SOC estimation methodologies in practical applications, e.g. embedded solutions in BMSs.

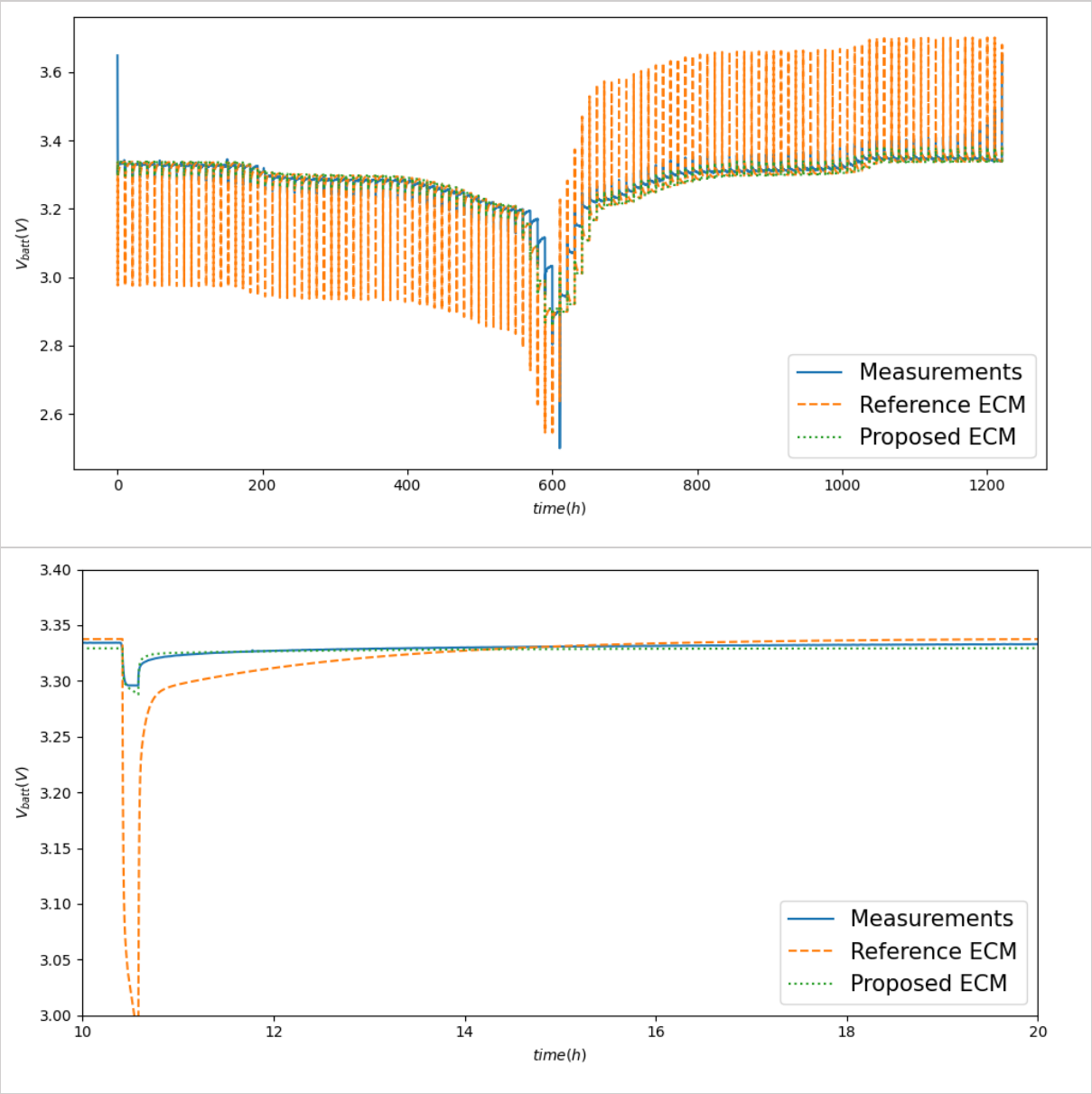

Fig 14: Comparison of the performances of the proposed ECM during GITT for a FRESH cell. From top to bottom: complete simulation results at, zoom of a current step followed by 10 hour relaxation.

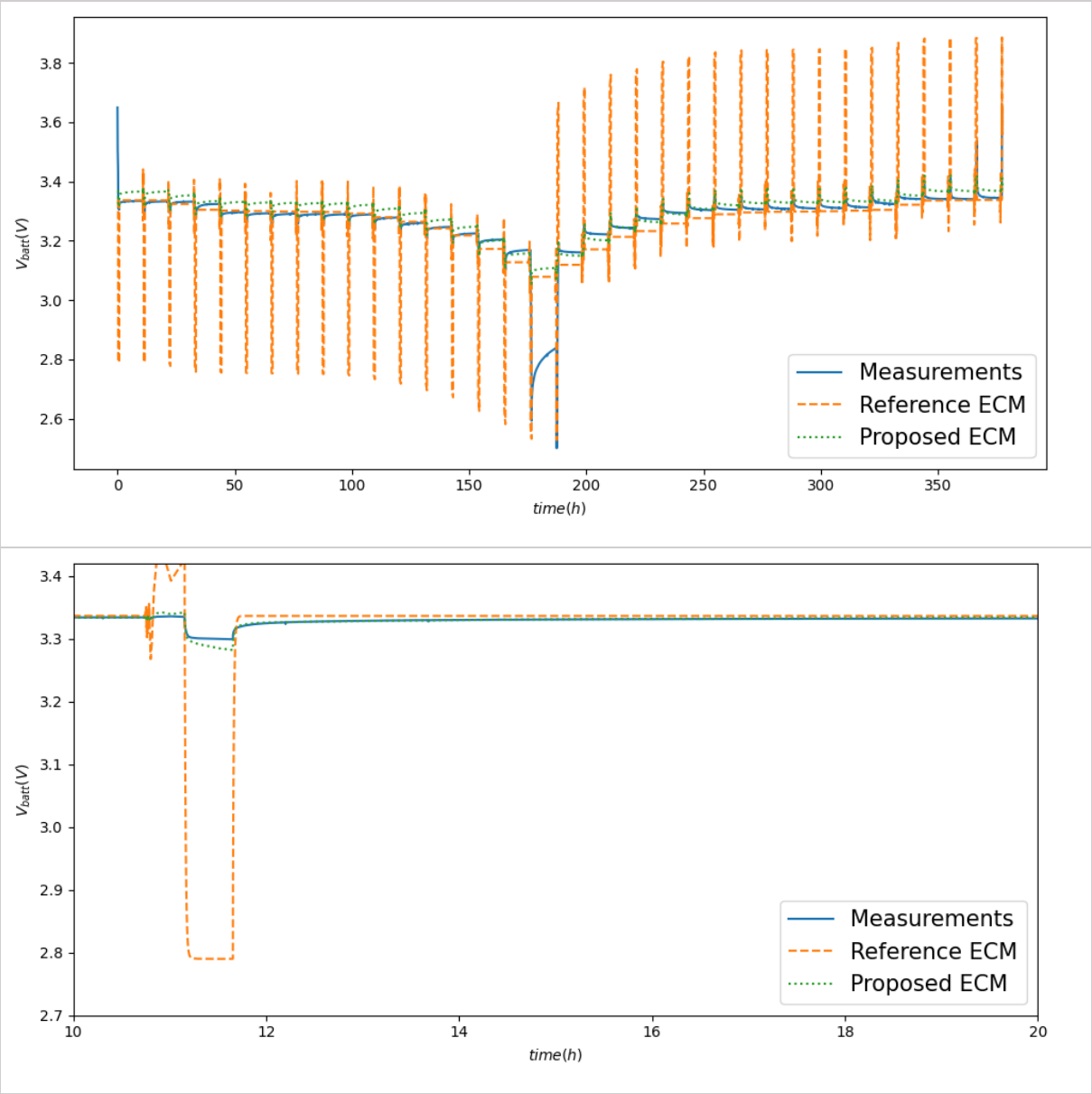

Fig 15: Comparison of the performances of the proposed ECM during GITT for a AGED cell. From top to bottom: complete simulation results at, zoom of a current step followed by 10 hour relaxation.

6 Outlook and next steps

The next steps can be divided according to their objectives:

To further enhance the accuracy of the model, it is crucial to acknowledge that EIS have been only measured at a specific SOC value of 50%. Recognizing that parameters are likely to be SOC-dependent, an extension of the model to cover the full SOC range becomes important, especially at extreme SoC levels, e.g. SoC < 5% and SoC > 95%. Moreover, temperature dependency of the models should be also addressed in the relevant range of common applications (-10°C – 45°C).

To further enhance the robustness of the model, it is suggested to investigate more in deep the proposed assumptions concerning the relationship between crystal lattice and relaxation time. This assumption should be subjected to validation through destructive measurements. Once confirmed, insights from existing literature can be leveraged to establish a clear correlation between chemical processes and ECM blocks can be established, possibly including ageing factors.

To further enhance the applicability of the model, it is advised to develop an estimation scheme for the very-low-frequency part of the EIS. Only in this way, the EIS-based solution proven in the hystimator project would find his implementation into embedded systems (e.g. into battery BMSs).

7 National and international cooperation

To enable a smooth transition for a post-project technology transfer, the creation of an external advisory board has been planned and executed. The advisory board has been organized such that the participants has been invited to two online meetings (24.08.2022 and 03.05.2023), where CSEM has informed about the status and results of the project. The participants for the advisory board are listed hereafter:

- BMW (OEM): Dr. Jiahao Li, Senior Researcher (Jiahao.Li@bmw.de)
- Gentherm (tier 1 supplier): Jason Chang, CTO (jason.chang@gentherm.com)
- Infineon (chip manufacturer): Dr. Günter Hofer, Concept Engineer for BMS (guenter.hofer@infineon.com)
- Green Cube (forklift products): Nicola Cinagrossi, Senior VP (ncinagrossi@greencubestech.com)
- Kyburz (mobility products): Olivier Groux, Head of R&D (olivier.groux@kyburz-switzerland.ch)
- Twice Energy (second life products): Philipp Strüby, CEO (philipp.strueby@twice-energy.ch)

The project HYSTIMATOR has been presented at the CSEM booth of the Electric Energy Storage EES 2023 (ees EUROPE 2023), which took place in June 2023 in Munich. CSEM has showcased a version of its zBMS demonstrator (Fig 16), which is based on the LFP cells investigated in the HYSTIMATOR projects.

Fig 16: CSEM's zBMS demonstrator showcase at the ees EUROPE 2023, equipped with the LFP cells used in HYSTIMATOR.

Finally, during the HYSTIMATOR projects effort have already been made to further develop projects in the frame of publicly financed innovation projects under the scheme of Horizon Europe projects. This will allow to continue pushing for different approach for SoC estimation of hysteresis-prone chemistries such as LFP.

8 Publications

Part of the results presented in this report have been published in the following conference paper:

G. Thenaisie, C. Brivio. Hystimator™: EIS-based hysteresis modelling of LFP cells, *8th International Conference on clean electrical power (ICCEP)*, 2023.

9 References

For the sake of simplicity, the references can be found in the pages' footnotes

10 Appendix: Test matrix

Test Protocol File	T chamber	Cell name	Cycler	Test ID	Event	Channel	Status	Short description	Machine time	Used
Cycling	Tamb	HYST_1_1	Arbin				Success	Cycling up to 1000 cycles 1C/1C	100	YES
0035_3_1_gittLONG_eis_LF90_AGED	20°C	HYST_1_1 (old LF90_1)	Biologic	0035	3_1	CD5	Fail	GITT + EIS (on AGED cell) (3h relaxation time)	7	NO
0035_3_2_gittLONG_eis_LF90_FRESH	20°C	HYST_2_2	Biologic	0035	3_2	CD6	Success	GITT + EIS (on FRESH cell) (3h relaxation time)	7	YES
0035_3_2_gitt_10min-10h_eis_LF90_FRESH	20°C	HYST_2_3	Biologic	0035	3_3	CD7	Success	GITT (10h relaxation time)	7	YES
0035_3_2_gitt_20min-5h_eis_LF90_FRESH	20°C	HYST_2_4	Biologic	0035	3_4	CD8	Success	GITT (5h relaxation time)	3.5	YES
LFP_2_5_10mHz_1p8A	20°C	HYST_2_5	Gamry			Sinlge ch.	Success	Short EIS 10mHz C/50	0	YES
0035_5_1_stepRELAX	20°C	HYST_2_5	Biologic	0035	5_1	CD5	Success	Step function and multiple days relaxation	24	YES
LFP_2_5_10uHz_1p8A_1	20°C	HYST_2_5	Gamry			Sinlge ch.	Success	Long EIS 10uHz C/50 #1	10	YES
0035_3_5_gitt_Vlevels_24h_LF90_HYST_2_4	20°C	HYST_2_4	Biologic	0035	3_5	CD8	Errror	GITT at chosed OCV levels (24h relaxation time)	20	NO
LFP_2_5_10uHz_1p8A_2	20°C	HYST_2_5	Gamry			Sinlge ch.	Success	Long EIS 10uHz C/50 #2	10	YES
LFP_2_5_10uHz_1p8A_3	20°C	HYST_2_5	Gamry			Sinlge ch.	Success	Long EIS 10uHz C/50 #3	10	YES
0035_3_6_gittLONG_30min-10h_withEIS_LF90_2_3	20°C	HYST_2_3	Biologic	0035	3_6	CD7	Success	GITT + intercalated EIS + 10h relax (on FRESH cell)	7	NO
0035_3_7_gittLONG_30min-10h_withEIS_LF90_1_1	20°C	HYST_1_1 (old LF90_1)	Biologic	0035	3_7	CD5	Success	GITT + intercalated EIS + 10h relax (on AGED cell)	7	NO
0035_6_1_validation_DYN_LF90_2_2	20°C	HYST_2_2	Biologic	0035	6_1	CD1-4	Success	DYN tests for model simulation/validation (3h relax)	1	YES
0035_6_2_validation_DYN_LF90_2_2	20°C	HYST_2_2	Biologic	0035	6_2	CD1-4	Success	DYN tests for model simulation/validation (10h relax)	1	YES
LFP_2_4_10mHz_1p8A	20°C	HYST_2_4	Gamry			Sinlge ch.	Success	Short EIS 10mHz C/50	0	YES
LFP_2_4_10mHz_0p9A	20°C	HYST_2_4	Gamry			Sinlge ch.	Success	Short EIS 10mHz C/100	0	YES
LFP_2_4_10uHz_0p9A_1	20°C	HYST_2_4	Gamry			Sinlge ch.	Errror	Long EIS 10uHz C/100 #1	10	NO
LFP_2_4_10uHz_0p9A_2	20°C	HYST_2_4	Gamry			Sinlge ch.	Success	Long EIS 10uHz C/100 #2	10	YES
LFP_2_4_10uHz_0p9A_3	20°C	HYST_2_4	Gamry			Sinlge ch.	Success	Long EIS 10uHz C/100 #3	10	YES
0035_3_8_gitt_1h-48h_LF90_2_3	20°C	HYST_2_3	Biologic	0035	3_8	CD7	Success	GITT (48h relaxation time)	20	YES
LFP_2_4_10uHz_0p9A_4(v_reg)	20°C	HYST_2_4	Gamry			Sinlge ch.	Success	Long EIS 10mHz C/100 #4	10	YES
LFP_1_1_100uHz_0p9A	20°C	HYST_1_1 (old LF90_1)	Gamry			Sinlge ch.	Success	Long EIS 100uHz C/100 #1	3	YES
0035_6_3_validation_DYN_LF90_2_2	20°C	HYST_2_2	Biologic	0035	6_3	CD5-8	Success	DYN tests for model simulation/validation (10h relax) --> 30' + 3h	0	NO
0035_6_4_validation_DYN_LF90_1_1	20°C	HYST_1_1 (old LF90_1)	Biologic	0035	6_4	CD5-8	Success	DYN tests for model simulation/validation (10h relax) --> 30' + 3h + shor	0	YES
									277.5	